The novel 2D-2D p-n heterojunction BiOBr/Bi$_{12}$O$_{15}$Cl$_6$ composites with enhanced visible light photocatalytic activity

DEYONG WU[*], HAIYAN TAN, CHENGYI WU
Hubei Key Laboratory of Biologic Resources Protection and Utilization, School of Chemical and Environmental Engineering, Hubei University for Nationalities, Enshi, 445000, China

The novel 2D-2D p-n heterojunction BiOBr/Bi$_{12}$O$_{15}$Cl$_6$ composites were formed by loading BiOBr nanosheets on the the surface of Bi$_{12}$O$_{15}$Cl$_6$ nanosheets. The samples were characterized by scanning electron microscopy, transmission electron microscopy, high-resolution transmission electron microscopy, energy dispersive spectrometer, X-ray diffraction and X-ray photoelectron spectroscopy. The obtained BiOBr/Bi$_{12}$O$_{15}$Cl$_6$ p-n heterojunction composites exhibited the superior photocatalytic activity for the degrading methyl orange under visible light irradiation as compared with Bi$_{12}$O$_{15}$Cl$_6$ and BiOBr, which should be mainly attributed to the formation of p-n heterojunction between Bi$_{12}$O$_{15}$Cl$_6$ and BiOBr, resulting in the higher quantum efficiency and stronger photocatalysis activity.

1. Introduction

Semiconductor photocatalysis has received more and more attention as an effective, green and potential technology for treating environmental pollutants[1-3]. Among these photocatalysts, the p-type bismuth oxychloride (BiOCl) is of great research interest, considering its high photocorrosion stability and good biocompatibility [4,5]. However, BiOCl has a 3.3 eV band gap, which greatly limits the practical application for solar energy conversion. Recently, adjusting the relative amounts of bismuth, oxygen and chloride was found as an effective way to decrease the band gap of bismuth oxychloride [6]. For example, Bi$_{12}$O$_{15}$Cl$_6$ has a narrow band gap of about 2.36 eV, and has exhibited excellent photocatalytic activity toward the degradation of Bisphenol A under visible light irradiation [7]. More interestingly, the intrinsic conductivity has been switched from p-type BiOCl to n-type Bi$_{12}$O$_{15}$Cl$_6$ [8]. For increasing the photocatalytic efficiency of Bi$_{12}$O$_{15}$Cl$_6$ photocatalyst, constructing heterostructure is an effective way, because the structures can considerably improve the electron-hole pair separation and interfacial charge transfer efficiency [9,10]. Especially, the p-n heterojunction, with an internal electric field in the interface, can significantly promote the separation of photogenerated charge carriers and further improve the degradation efficiency [11,12]. The p-type bismuth oxybromide (BiOBr) has been reported to couple with other semiconductors to form heterojunction photocatalyst, such as Ag$_3$PO$_4$/BiOBr [13], Bi$_2$O$_3$/BiOBr [14], SrTiO$_3$/BiOBr [15]. To the best of our knowledge, there are no existing reports on the preparation and investigation of p-BiOBr/n-Bi$_{12}$O$_{15}$Cl$_6$ system. Herein, we report novel heterojunction of p-type BiOBr and n-type Bi$_{12}$O$_{15}$Cl$_6$ constructed by loading BiOBr nanosheets on the surface of BiOBr nanosheets. The photocatalytic activity of the p-BiOBr/n-Bi$_{12}$O$_{15}$Cl$_6$ heterojunction photocatalysts was evaluated by degrading MO under visible light irradiation.

2. Experimental

2.1. Synthesis of the photocatalysts

All the chemical was analytical grade and used without further purification. Bi$_{12}$O$_{15}$Cl$_6$ Nanosheets was prepared according to the reported method [7]. In a typical synthesis, 2 mmol Bi(NO$_3$)$_3$·5H$_2$O was added into 20 mL ethylene glycol (EG), and the mixture was dispersed to form a homogeneous solution under vigorous stirring. Meanwhile, 0.66 mmol NH$_4$Cl was added to 70 mL distilled water while vigorously stirring to form a homogeneous solution. Then, the above two solutions were mixed, and transferred to a 100 mL autoclave with a Teflon liner. It was heated at 160 °C for 12 h, and then allowed to cool to room temperature. The resulting powder was collected via centrifugation and washed with distilled water and alcohol three times to remove the residual ions. The products were dried at 80 °C for 6 h and then calcined in the Muffle Furnace at 400 °C for 5 h.

The preparation of BiOBr/Bi$_{12}$O$_{15}$Cl$_6$ composites were as follows: 1mmol Bi(NO$_3$)$_3$·5H$_2$O was added into 35 mL EG to form a clear solution A under vigorous stirring, and 1mmol KBr was added into 35 mL EG to form a clear solution B under vigorous stirring. Then, Solution A was added into Solution B under magnetic stirring to form a homogeneous solution under magnetic stirring for 30 min.

Afterwards, 0.5 g $Bi_{12}O_{15}Cl_6$ was dispersed into the above homogeneous solution under the ultrasonic assistance for 30 min. After that, the suspension was transferred into a 100 ml Teflon-lined autoclave, and heated to 160 °C for 24 h, and cooled to room temperature naturally. The obtained $BiOBr/Bi_{12}O_{15}Cl_6$ composites were washed by distilled water and ethanol several times, finally dried at 80 °C for 12 h.

As a control, BiOBr was also prepared from the above system in the absence of $Bi_{12}O_{15}Cl_6$ through the solvothermal route at 160 °C for 24 h.

2.2. Characterization of catalysts

X-ray powder diffraction (XRD) pattern of samples were recorded on a powder X-ray diffractometer (D/max-2200/PC, Rigaku Corporation, Japan) with Cu Ka radiation, operating at 40 kV and 30 mA, where λ=0.15418 nm for the Cu Kα radiation. XPS experiments were carried out on a RBD upgraded PHI-5000C ESCA system (Perkin Elmer, USA), the shift of the binding energy due to relative surface charging was corrected using the C 1s level at 284.6 eV as an internal standard. The structure and morphology of the coatings were investigated by the field emission scanning electron microscopy (FESEM, FEI SIRION 200, FEI, USA) and the transmission electron microscopy (TEM, JEM-100CX, JEOL, Japan).
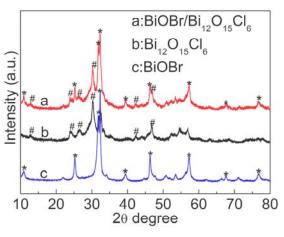
2.3. Photocatalytic evaluation studies

The photocatalytic activity of the catalysts was evaluated by degradation of methyl orange (MO) under visible light irradiation. A 300 W Xe lamp was used as the light source of a homemade photoreactor, surrounded with a water circulation facility at the outer wall through a quartz jacket. The 420 nm cut off filter was used to get the visible light source. In each experiment, 0.05 g of the as-prepared photocatalyst was added into 50 mL of MO solution (20 mg/L). Before irradiation, the suspensions were placed in dark and stirred for 30 min to achieve adsorption equilibrium. Subsequently, MO solution was sampled at every interval and the residual MO concentration was monitored at 464 nm using a UV-vis spectrophotometer (UNICO 7200).

3. Results and discussion

Fig. 1 shows XRD patterns of $BiOBr/Bi_{12}O_{15}Cl_6$ composites, pure $Bi_{12}O_{15}Cl_6$ and BiOBr. All the characteristic diffraction peaks in Fig. 1b could be assigned to the tetragonal phase of $Bi_{12}O_{15}Cl_6$ (JCPDS card No. 70-0249) [7]. All the identified peaksin Fig. 1c can be perfectly assigned to the tetragonal phase of BiOBr (JCPDS card No. 09-0393)[16]. Structurally, the $BiOBr/Bi_{12}O_{15}Cl_6$ heterojunctions present a two-phase composition, i.e., the tetragonal phase of BiOBr and the

tetragonal phase of $Bi_{12}O_{15}Cl_6$, with no other impurity peaks from the diffraction patterns.

Fig. 1. XRD patterns of pure $Bi_{12}O_{15}Cl_6$, BiOBr and $BiOBr/Bi_{12}O_{15}Cl_6$ composites

The morphologies of $Bi_{12}O_{15}Cl_6$, BiOBr and $BiOBr/Bi_{12}O_{15}Cl_6$ composites were observed by SEM and TEM images. As shown in Fig. 2a and Fig. 2c, $Bi_{12}O_{15}Cl_6$ is composed of lots of irregular nanosheets with smooth surfaces. Furthermore, it was observed easily that $Bi_{12}O_{15}Cl_6$ nanosheets are nearly transparent, which indicates their ultrathin thickness. Fig. 2b and Fig. 2d displayed the morphologies of $BiOBr/Bi_{12}O_{15}Cl_6$ composites. It was found easily that the 2D BiOBr nanosheets are dispersed on the 2D $Bi_{12}O_{15}Cl_6$ thin nanosheets. In facts, the pure BiOBr presented spherical microstructures consisted of abundant nanosheets with several nanometers in thickness, as shown in Fig. 3. It may be attributed to the fact that the existence of $Bi_{12}O_{15}Cl_6$ inhibit the formation of BiOBr microspheres. Similar observation has been reported in previous literature [17]. To prove the formation of $BiOBr/Bi_{12}O_{15}Cl_6$ heterojunctions, the EDS technology was employed. As shown in Fig. 4, it is obvious that major peaks are indexed to copper (copper signals are from the copper grid), carbon (carbon signals are from contaminant carbon), oxygen, bromine, chlorine and bismuth respectively, which can verify that the fabricated sample consist of BiOBr and $Bi_{12}O_{15}Cl_6$. In addition, an interface between BiOBr and $Bi_{12}O_{15}Cl_6$ can be observed in the HRTEM image (Fig. 5). Observing both sides of the interface, the lattice fringes at 0.31 and 0.28 nm coincide with the fringe spacing of the (413) lattice plane of $Bi_{12}O_{15}Cl_6$ [7] and the (110) crystal plane of BiOBr [18], respectively. This result further confirmed the co-existence of BiOBr and $Bi_{12}O_{15}Cl_6$ in the composite. The obvious interface between BiOBr and $Bi_{12}O_{15}Cl_6$ implies the formation of a heterojunction structure.
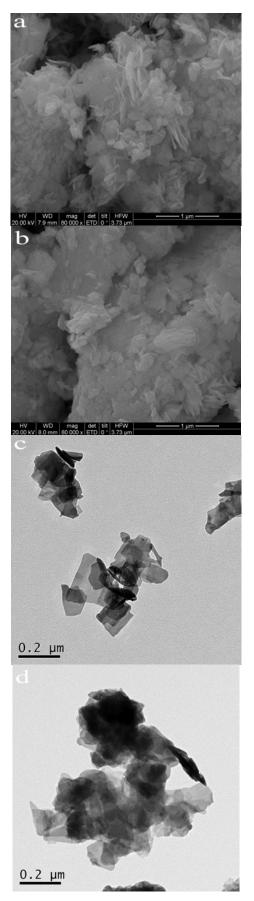
Fig. 2. SEM images of (a) pure Bi$_{12}$O$_{15}$Cl$_6$ and(b) BiOBr/Bi$_{12}$O$_{15}$Cl$_6$ composites. TEM images of (c) pure Bi$_{12}$O$_{15}$Cl$_6$ and (d) BiOBr/Bi$_{12}$O$_{15}$Cl$_6$ composites
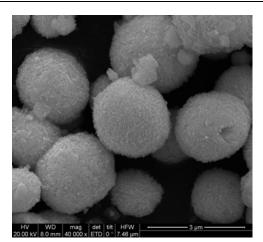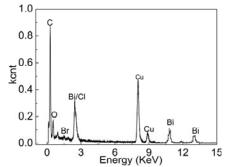

Fig. 3. SEM images of as-prepared BiOBr spherical microstructures

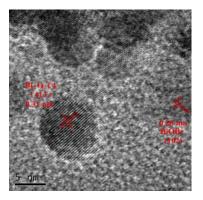*Fig. 4. EDS pattern of BiOBr/Bi$_{12}$O$_{15}$Cl$_6$ photocatalyst*

Fig. 5. HRTEM image of BiOBr/Bi$_{12}$O$_{15}$Cl$_6$ c omposites

XPS measurements were performed to investigate the composition and chemical states of BiOBr/$Bi_{12}O_{15}Cl_6$ composites. The relevant XPS peak position is calibrated against the C1s signal of contaminant carbon at a binding energy of 284.6 eV. The Br 3d XPS spectrum (Fig.6a) showed two main peaks with binding energies at 68.4 eV and 69.5 eV, corresponding to the Br $3d_{5/2}$ and Br $3d_{3/2}$, respectively [19]. As for the spectra of Cl 2p (Fig. 6b), the peaks located at 198.2 eV and 199.7 eV, ascribing to the binding energies of Cl $2p_{3/2}$ and Cl $2p_{1/2}$, respectively [20]. In addition, the Bi 4f XPS spectrum were showed in Fig. 6c, two main peaks with binding energies at 159.3 eV and 164.6eV were ascribed to the Bi $4f_{7/2}$ and Bi $4f_{5/2}$, respectively [21].
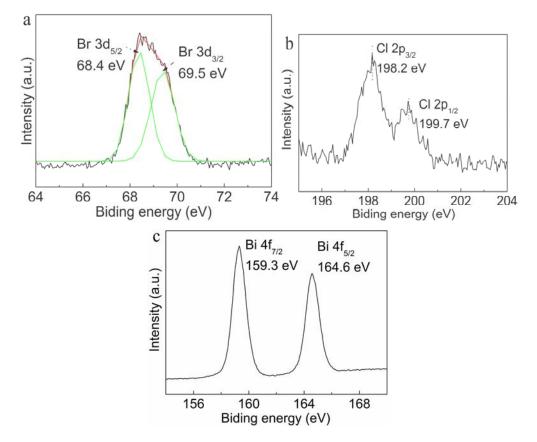

Fig. 6. XPS spectra of Br 3d (a), Cl 2p (b) and of the BiOBr/$Bi_{12}O_{15}Cl_6$ composites

The photocatalytic activities of $Bi_{12}O_{15}Cl_6$, BiOBr and BiOBr/$Bi_{12}O_{15}Cl_6$ composites for degradation of MO under visible light irradiation were displayed in Fig.7a. From the degradation results, $Bi_{12}O_{15}Cl_6$ and BiOBr have visible-light-induced photocatalytic activity, because they possesses efficient visible light absorption. And $Bi_{12}O_{15}Cl_6$ and BiOBr could degradate 25.8 % and 48.1% MO in 180 min, respectively. However, the BiOBr/$Bi_{12}O_{15}Cl_6$ composites exhibited higher photocatalytic activity under identical experimental conditions. The BiOBr/$Bi_{12}O_{15}Cl_6$ composites degraded nearly 63.0% MO in 180 min. Generally, the photocatalytic degradation of MO could be considered as a pseudo-first-order reaction with low concentration, and its kinetics could be expressed as the formula $\ln(C/C_0) = -k\,t$, where C_0 and C are the initial concentration of MO and the concentration of pollutant at a reaction time of t, respectively, k is the degradation rate constant [22]. A good linear relationship was observed between $-\ln(C/C_0)$ and irradiation time, as shown in the Fig. 7b. The MO degradation rate constants were calculated as 0.00153, 0.00378 and 0.0056 min^{-1} for $Bi_{12}O_{15}Cl_6$, BiOBr and BiOBr/$Bi_{12}O_{15}Cl_6$, respectively. The outstanding photocatalytic activity of BiOBr/$Bi_{12}O_{15}Cl_6$ should be attributed to the formation of p-n heterojunction between $Bi_{12}O_{15}Cl_6$ and BiOBr, because the p-n heterojunctions can facilitate the separation of electrons and holes, resulting in the higher quantum efficiency and stronger photocatalysis activity [23]. According to the ref. [24] and ref. [7], the E_{VB} values of BiOBr and $Bi_{12}O_{15}Cl_6$ were 2.98 and 1.85 eV, and the E_{CB} values of them were 0.39 and -0.51 eV, respectively. The band edge positions of BiOBr and $Bi_{12}O_{15}Cl_6$ showed a nested band structure as schematically illustrated in Fig. 8a. When p-type BiOBr is in contact with n-type $Bi_{12}O_{15}Cl_6$ to form a p-n heterojunction, the Fermi levels of p-BiOBr and n-$Bi_{12}O_{15}Cl_6$ are aligned under thermal equilibrium conditions [24], as shown in Fig. 8b. Under visible light irradiation, BiOBr and $Bi_{12}O_{15}Cl_6$ all can be excited to generate electron-hole pairs. According to the band edge position, the excited electrons on the CB of p-type BiOBr transfer to that of n-type $Bi_{12}O_{15}Cl_6$ and the excited holes

on the VB of n-type Bi$_{12}$O$_{15}$Cl$_6$ transfer to that of p-type BiOBr. Meanwhile, the migration of photogenerated carriers was promoted by the internal electric field with direction from the n-type Bi$_{12}$O$_{15}$Cl$_6$ to the p-type BiOBr. In this way, the recombination of electron-hole pairs was remarkably reduced. As a result, the BiOBr/Bi$_{12}$O$_{15}$Cl$_6$ composites exhibit better photocatalytic activity than those of pure Bi$_{12}$O$_{15}$Cl$_6$ and BiOBr for the degradation of MO under visible light irradiation.
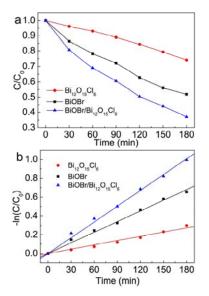

Fig. 7. Photocatalytic degradation of (a) MO (initial concentration of 20 mg/L) in the presence of as-prepared samples under visible light irradiation. (b) Linear transform -ln(C/C$_0$) = kpt of   the kinetic curves for MO degradation by different samples
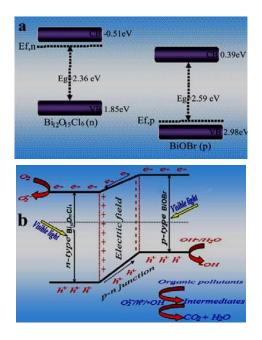

Fig. 8. Diagram of the band energy of Bi$_{12}$O$_{15}$Cl$_6$ (a) and BiOBr before contact and (b) formation of a p-n junction and the proposed charge separation process of BiOBr/Bi$_{12}$O$_{15}$Cl$_6$ heterostructures   under visible light irradiation

4. Conclusions

In summary, the novel 2D-2D p-n heterojunction BiOBr/Bi$_{12}$O$_{15}$Cl$_6$ composites were formed by loading BiOBr nanosheets on the surface of Bi$_{12}$O$_{15}$Cl$_6$ nanosheets. Compared to pure Bi$_{12}$O$_{15}$Cl$_6$ and BiOBr photocatalysts, the BiOBr/Bi$_{12}$O$_{15}$Cl$_6$ composites displayed higher photocatalytic performance for the photodegradation of MO under visible light irradiation, which can be attributed to the formation of a heterojunction electric field on the interface between BiOBr and Bi$_{12}$O$_{15}$Cl$_6$. The existence of this electric field can effectively inhibit the recombination of the photogenerated electrons and holes and thus can dramatically enhance the photocatalytic MO degradation performance.

References

[1] A. Tolosana-Moranchel, J. A. Casas, J. Carbajo, et al., Appl. Catal. B-Environ. **200**, 164 (2017).
[2] A. Bachvaiova-Nedelcheva, R. Iordanova, A. Stoyanova, et al., J. Optoelectron. Adv. M. **18**(1-2), 5 (2016).
[3] A. C. Cakir, P. Guloglu, M. Bilgin, et al., J. Optoelectron. Adv. M. **14**(3-4), 230 (2012).
[4] D. J. Mao, A. Q. Yu, S. S. Ding, et al., Appl. Surf. Sci. **389**, 742 (2016).
[5] C. Hao, Y. M. Xu, M. J. Bao, et al., J. Mater. Sci-Mater El. **28**(4), 3119 (2017).
[6] X. Xiao, C. Liu, R. P. Hu, et al., J. Mater. Chem. **22**(43), 22840 (2012).
[7] C. Y. Wang, X. Zhang, X. N. Song, et al., ACS Appl. Mat. Interfaces **8**(8), 5320 (2016).
[8] Y. Myung, F. Wu, S. Banerjee, et al., Chem. Mater. **27**(22), 7710 (2015).
[9] F. Zheng, D. Wu, J. Xia, et al., J. Optoelectron. Adv. M. **17**(9-10), 1528 (2015).
[10] L. F. Li, P. P. Xiao, M. L. Zhang, et al., J. Optoelectron. Adv. M. **18**(5-6), 521 (2016).
[11] Y. H. Wang, Y. X. Deng, L.G. Fan, et al., RSC Adv. **7**(39), 24064 (2017).
[12] J. X. Low, J. G. Yu, M. Jaroniec, et al., Adv. Mater. **29** (20), 1601694 (2017).
[13] O. Mehraj, N. A. Mir, B. M. Pirzada, Appl. Surf. Sci. **32**, 419 (2015).
[14] A. J. Han, J. L. Sun, G. K. Chuah, et al., RSC Adv. **7**(1), 145 (2017).
[15] T. Kanagaraj, S. Thiripuranthagan, Appl. Catal. B-Environ. **207**, 218 (2017).
[16] A. C. Mera, H. Valdes, F. J. Jamett, et al., Solid State Sci. **65**, 15 (2017).

[17] Y. H. Ao, K. D. Wang, P. F. Wang, et al., Appl. Catal. B-Environ. **194**, 157 (2016).
[18] X.Yu, J. J.Shi, L.J.Feng, et al., Appl. Surf. Sci. **396**, 1775 (2017).
[19] F. Z. Qiu, W. J. Li, F. Z. Wang, et al., J. Colloid Interface Sci. **493**, 1 (2017).
[20] Q. H. Zhao, X. Y. Liu, Y.X. Xing, et al., J. Mater. Sci. **52**(4), 2117 (2017).

[21] Z. J. Li, Y. Qu, K. Hu, et al., Appl. Catal. B-Environ. **203**, 355 (2017).
[22] T. He, D. Wu, J. Mater. Sci-Mater El. **28**(10), 7320 (2017).
[23] X. C. Meng, Z. S. Zhang, Mater. Lett. **189**, 267 (2017).
[24] F. Z. Qiu, W. J. Li, F. Z. Wang, et al., Colloid Surface A **517**, 25 (2017).

*Corresponding author: wdy001815@126.com